

# Geomechanical behavior of $\text{CO}_2$ storage in Saline Aquifers (GeoCoSA): benchmark problem description

Sarah Gasda<sup>1</sup>, Melanie Darcis<sup>2</sup>, Mark White<sup>3</sup>, Bernd Flemisch<sup>2</sup>,  
and Holger Class<sup>2</sup>

<sup>1</sup>Center for Integrated Petroleum Research, Uni Research, Bergen, Norway

<sup>2</sup>Institut für Wasser- und Umweltsystemmodellierung (IWS), Universität Stuttgart,  
Germany

<sup>3</sup>Pacific Northwest National Laboratory, Richland, Washington, USA

May 27, 2013

## Introduction

Geological sequestration of  $\text{CO}_2$  is an increasingly attractive option for sequestering large amounts of anthropogenic  $\text{CO}_2$  emissions. The success of this technology relies on safe injection of  $\text{CO}_2$  into the deep subsurface with minimal impact on human health and environmental resources. To this end, reliable computational models are needed to assess and manage risk associated with injection operations.

Computational models have been used extensively to study multiphase problems in petroleum and hydrological engineering. Despite the confidence gained from decades of experience in modeling fluid flow porous media, the problem of  $\text{CO}_2$  sequestration brings added complexity not always found in other multiphase flow systems. For instance,  $\text{CO}_2$  injection will increase in-situ pore pressure and may result in significant geomechanical stresses and subsequent deformation of the host rock [3]. This may result in unintended consequences such as fracturing, fault activation and induced seismicity, which are a concern for large-scale injection projects. Coupled geomechanical and fluid flow processes increases model complexity, and therefore simulation codes need to be thoroughly benchmarked against known solutions, field data and other codes within the modeling community.

While several benchmark and inter-comparison model studies have been carried out in the  $\text{CO}_2$  modeling community [4, 6, 7], none have focused exclusively on geomechanical deformation induced by  $\text{CO}_2$  injection. The single geomechanics benchmark included in [7] had only one participant, and therefore no model

comparisons were made. Thus, there is evident need for a model comparison study dedicated to geomechanics associated with CO<sub>2</sub> storage systems.

One purpose of this comparison is to build confidence in existing simulators to reliably model geomechanical behavior for different CO<sub>2</sub> injection problems. However, given the complexity of hydrogeomechanical processes in real systems, different simulators will approach the problem with a certain set of assumptions or model simplifications. Therefore, another goal of this study is to understand the impact of these modeling approaches on the model solution and quantify the resulting uncertainty.

## 1 Problem 1

### 1.1 Problem Definition

#### System geometry

The system is defined as a single permeable storage aquifer bounded on top and bottom by a relatively impermeable overburden and underburden, respectively. The system has a lateral extent of 10 kilometers and total thickness of 4000 m. The overburden is split into shallow and deep overburden. The shallow overburden extends from the ground surface to a flat surface 900 mbs (meters below surface). The deep overburden extends from 900 mbs to the top boundary of the aquifer at 1800 mbs. The storage aquifer has a uniform thickness of 20 m. The underburden extends from the bottom aquifer boundary (1820 mbs) to a depth of 4000 mbs.

#### Boundary and Initial conditions

The flow boundary conditions are fixed pressure and saturation at the outer and top boundaries. The bottom boundary is a zero flux condition. Zero displacement is set at the lateral and bottom boundaries and free at the top boundary.

The system is initially filled with formation fluid (brine) at hydrostatic pressure. The initial pressure at the reservoir top is 17.9 MPa and temperature is 90° C.

The initial stress condition is an idealized isotropic in-situ stress field with one principal stress pointing in vertical direction. The magnitude of the principal in-situ stresses ( $\sigma_1$ ,  $\sigma_2$ ,  $\sigma_3$ ) is the lithostatic pressure determined as a function of depth

$$\sigma_1 = \sigma_2 = \sigma_3 = \phi \rho_f D + (1 - \phi) \rho_s D. \quad (1)$$

With the porosity  $\phi$ , the pore fluid density  $\rho_f$ , the rock matrix density  $\rho_s$  and the depth below surface  $D$ .

#### Injection

CO<sub>2</sub> is injected into the storage through a vertical well at the horizontal center of the domain. The injection is spread across the entire thickness of the aquifer,

Table 1: Rock properties

<i>Layer</i>	<i>Permeability</i> (mD)	<i>Porosity</i> (%)	<i>Young's</i> <i>modulus</i> (GPa)	<i>Poisson's</i> <i>ratio</i>
Shallow overburden	0.01	10	1.5	0.2
Deep overburden	0.0001	10	20	0.15
Storage aquifer	13	17	6	0.2
Underburden	0.0001	10	20	0.15

and the well radius is 0.05 m. The injection rate is constant at 40,000 tons/yr at 90° C for 3 years. There is no shut-off period.

### Formation properties

The rock properties assigned to each layer are given in Table 1. The properties are homogeneous within each individual layer. The rock thermal conductivity in each layer is 3 W/(m·K), specific heat is 0.92 kJ/kg K, and the rock specific gravity 2.5.

### Fluid properties

Fluid properties can be based on any typical PVT model of choice. The relative permeability and capillary pressure relationships are the classical Brooks-Corey curves [2] for brine,

$$k_w = (S_{wn})^\lambda \quad (2)$$

and CO<sub>2</sub>

$$k_c = 0.4(1 - S_{wn}^{\frac{\lambda}{2}})(1 - S_{wn})^{\frac{\lambda}{2}} \quad (3)$$

where  $\lambda = 4$ ,  $S_{wn}$  is the normalized brine saturation with irreducible water saturation set  $S_{wr} = 0.3$ . Primary drainage capillary pressure is given by

$$P_c = p_d(S_{wn})^{-\frac{1}{m}} \quad (4)$$

with  $p_d = 0.2$  bar and exponent  $m = 2$ .

### Rock mechanics

Geomechanical deformation may be modeled using any approach to elastic and/or plastic deformation. In addition, there is no prescribed approach to coupling with fluid flow. Porosity and/or permeability changes with respect to stress may be considered.

If failure potential is evaluated, then the following conditions apply in the whole model domain—the angle of internal friction  $\varphi$  is 30°, while the internal cohesive force  $S_0$  and the tensile strength are set to zero.

## 1.2 Model Comparison Reporting

The following measures should be reported in tabulated files with accompanying figures.

### Vertical displacement

The vertical displacement at three depths—1) the ground surface (0 mbs); 2) at the reservoir top (1800 mbs); and 3) at the reservoir bottom (1820 mbs)—should be reported in the following ways:

- maximum displacement (positive or negative) in time over a 3-year period;
- location of maximum displacement;
- spatial distribution ( $x$ - $y$ ) of vertical displacement at 3 years.

In addition, the vertical displacement at three years in an  $x - z$  cross-section of the whole domain (0-4000 mbs) through the well location should also be reported.

### Porosity and permeability changes

Porosity and permeability changes (as a percent increase/decrease from original values) in the reservoir (1810 mbs) should be reported in the following ways:

- maximum change in time over a 3-year period;
- location of maximum change;
- $x$ - $y$  spatial distribution of percent change at 3 years.

### CO<sub>2</sub> saturation and pressure

CO<sub>2</sub> saturation should be reported at 3 years as an  $x$ - $z$  cross-section of the reservoir through the well location. Pressure should be reported in time at the wellhead and as a  $x$ - $y$  spatial distribution at the reservoir top at 3 years.

### Effective stress

Spatial distributions of the changes in effective stresses ( $\Delta\sigma'_z$ ,  $\Delta\sigma'_x$ ,  $\Delta\sigma'_y$ ) due to CO<sub>2</sub> injection should be given at the reservoir top (in  $x$ - $y$ ) and at the well location (in  $x$ - $z$ ) after 3 years.

### Failure potential

It should be discussed if there is a potential for rock failure due to CO<sub>2</sub> injection. The  $x$ ,  $y$  and  $z$  ranges within which rock failure is most probable and the method of failure potential evaluation should be reported.

As an example, the failure potential could be evaluated based on pressure margins for tensile failure  $p_{fm}$  and for shear failure  $p_{sm}$  as proposed by [? ]. If the pressure margin becomes equal or larger than zero, there is a potential for rock failure.

The pressure margin for tensile failure is calculated as a function of the critical fluid pressure for hydraulic fracturing  $p_{fc}$

$$p_{fc} = \sigma_3, \quad (5)$$

$$p_{fm} = p - p_{fc}. \quad (6)$$

$\sigma_3$  represents the least principal stress component,  $p$  is the fluid pressure.

The pressure margin for shear failure is a function of the critical fluid pressure for the onset of slip  $p_{sc}$

$$p_{sc} = \left( \sigma_m - \frac{|\tau_m| - S_0 \cos \varphi}{\sin \varphi} \right), \quad (7)$$

$$p_{sm} = p - p_{sc}. \quad (8)$$

With the mean principal stress  $\sigma_m = (\sigma_3 + \sigma_1)/2$  and the maximum shear stress  $\tau_m = (\sigma_1 - \sigma_3)/2$ .

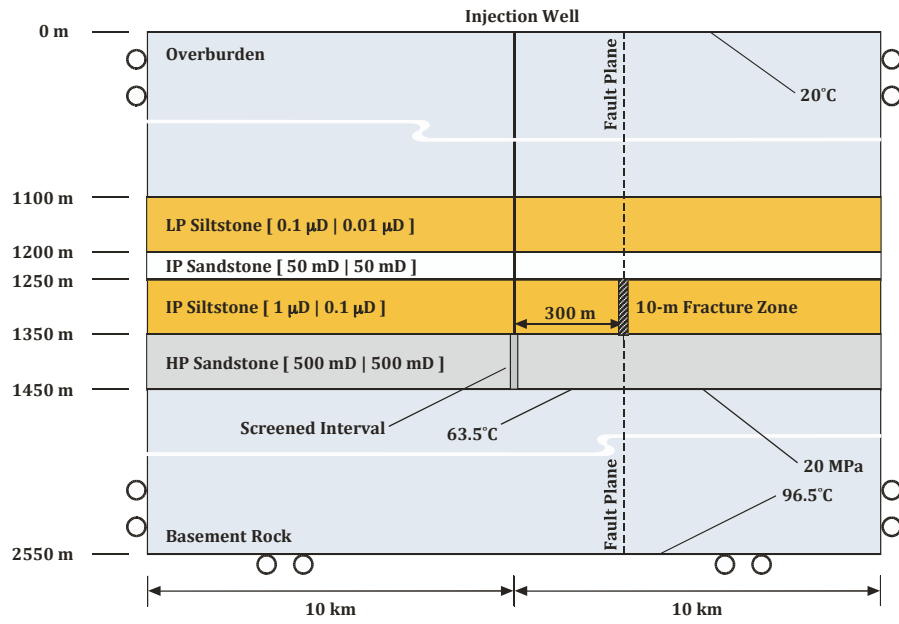
## 2 Problem 2

### 2.1 Problem definition

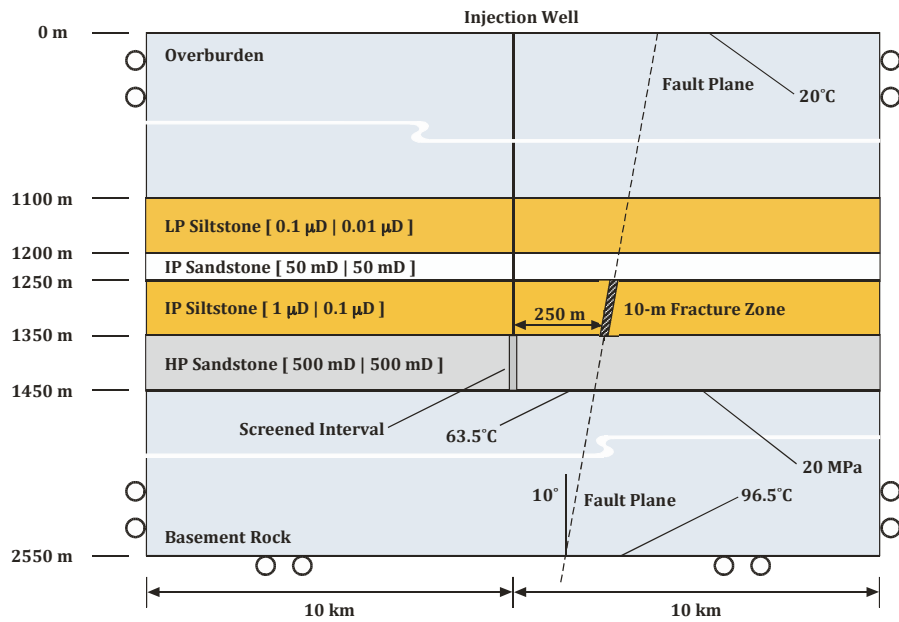
The geologic system is an idealized structure, shown in Figure 1, that comprises four horizontal layers starting from the ground surface: 1) 1100-m overburden of impermeable rock; 2) 100-m secondary caprock of lower permeability siltstone; 3) 50-m secondary saline reservoir of intermediate permeability sandstone; 4) 100-m primary caprock of intermediate permeability siltstone; 5) 100-m primary saline reservoir of high permeability sandstone; and 6) 1150-m impermeable basement rock. The computational domain is a two-dimensional slice through the geology with a 1-m thickness. The lateral extent of the domain is 20 km and the overall vertical extent is 2600 m. A vertical CO<sub>2</sub> injection well is located at the lateral center of the domain, with a screened interval across the primary saline reservoir. A discrete fault plane with a 10-m thickness transects the computational domain. The fault can be modeled in one of two ways: 1) as a tilted fault with an angle 10° from the vertical and located 250 m from the injection well; or 2) as a vertical fault located 300 m from the injection well. See Figures 1a and 1b for a detailed schematic of the two options. Associated with this fault plane is a 10-m thick fracture zone within the primary caprock.

### Boundary and Initial Conditions

All boundaries are closed to fluid flow. For geomechanics the lower domain boundary is a zero vertical displacement boundary, the lateral domain boundaries are zero horizontal displacement boundaries, and the upper domain boundary is a free displacement boundary. The hydrologic system is assumed to be



(a) Vertical fault



(b) Tilted fault

Figure 1: Schematic of domain and associated properties for Problem 2 with two options for the fault plane angle: 1) vertical and 2) tilted at 10° angle from vertical.

under hydrostatic pressure conditions with a uniform salt mass fraction in the brine of 0.1. The pressure at the bottom of the primary reservoir (i.e., 1500 mbgs) is assumed to be 20 MPa. A geothermal gradient of  $-0.03^{\circ}\text{C}/\text{m}$  is assumed with an initial temperature of  $65^{\circ}\text{C}$  at the bottom of the primary reservoir (i.e., 1500 mbgs). The surface temperature is maintained at  $20^{\circ}\text{C}$  and the lower boundary surface temperature at a depth of 2600 m is maintained at  $98^{\circ}\text{C}$ . Three different initial stress states will be considered: 1) compressive stress state with the initial horizontal stress equal to 1.5 times the vertical lithostatic stress ( $\sigma_h = 1.5 \sigma_v$ ); 2) isotropic stress state with the initial horizontal stress equal to the vertical lithostatic stress ( $\sigma_h = \sigma_v$ ); and 3) extensive stress state with the initial horizontal stress equal to 0.75 times the vertical lithostatic stress ( $\sigma_h = 0.75 \sigma_v$ ). The lithostatic stress is determined from the rock saturated density.

### Injection

Pure  $\text{CO}_2$  is injected for 30 years at a constant rate of 0.04 kg/s over the entire screened interval for the 1-m thickness of the computational domain. The well radius is 0.15 m and no injection pressure limit is imposed on the well. The injection temperature at the screened interval is  $40^{\circ}\text{C}$ , making the injected fluid within the supercritical gas region for  $\text{CO}_2$ .

### Rock Hydrological Properties

The modeled system comprises four permeable rocks: 1) HP Sandstone, 2) IP Sandstone, 3) IP Siltstone, and 4) LP Siltstone; and two relatively impermeable rocks: 1) Overburden and 2) Basement Rock. The sandstones and impermeable rocks are assumed to have isotropy intrinsic permeability; whereas, the siltstone has anisotropic intrinsic permeability with a horizontal to vertical ratio of 10:1. Shear strain and reactivation of the fault plane is not considered in this problem.

#### *Fractured rock*

The fracture zone, associated with the fault plane, is assumed to comprise a two-dimensional array of homogeneous orthogonal fractures, oriented longitudinally and transversely to the fault plane. The longitudinal fractures are oriented parallel to the fault plane and the tranverse fractures are oriented perpendicular to the fault plane. The fracture zone intrinsic permeability is computed as a function of the normal stress on the fractures, through permeability correction factors (longitudinal,  $F_{lfr}^k$ , and transverse,  $F_{tfr}^k$ ) to the initial fracture intrinsic permeabilities (longitudinal,  $k_{lfr}^i$ , and transverse,  $k_{tfr}^i$ ) [9]:

$$\begin{aligned} k_h &= k_{lfr}^i F_{lfr}^k \sin \theta + k_{tfr}^i F_{tfr}^k \cos \theta \\ k_v &= k_{lfr}^i F_{lfr}^k \cos \theta - k_{tfr}^i F_{tfr}^k \sin \theta \end{aligned} \quad (9)$$

where  $\theta$  is the fault tilt from vertical. The longitudinal and transverse permeability correction factors are computed from the current and initial fracture apertures,  $b$  and  $b^i$ , using the cubic law:

$$\begin{aligned}
F_{lfr}^k &= \frac{(b_l)^3}{(b_l^i)^3} \\
F_{tfr}^k &= \frac{(b_t)^3}{(b_t^i)^3}
\end{aligned} \tag{10}$$

The current fracture aperture is computed from the initial fracture aperture ( $b^i$ ), maximum fracture aperture ( $b^{\max}$ ), initial normal stress ( $\sigma^i$ ), and current normal stress ( $\sigma'$ ), for both longitudinal and transverse directions:

$$\begin{aligned}
b_l &= b_l^i + b_l^{\max} (\exp(d\sigma'_l) - \exp(d\sigma_l^i)) \\
b_t &= b_t^i + b_t^{\max} (\exp(d\sigma'_t) - \exp(d\sigma_t^i))
\end{aligned} \tag{11}$$

where  $d$  is the fracture stress model parameter.

The fracture zone porosity is also computed from an initial fracture porosity ( $\phi_{fr}^i$ ) and a porosity correction factor ( $F_{fr}^\phi$ ):

$$\phi_{fr} = F_{fr}^\phi + \phi_{fr}^i \tag{12}$$

The porosity correction factor  $F_{fr}^\phi$  is computed from the current and initial fracture apertures in the longitudinal and transverse directions:

$$F_{fr}^\phi = \frac{(b_l + b_t)}{(b_l^i + b_t^i)} \tag{13}$$

The fracture zone capillary pressure is also computed from an initial capillary pressure and a capillary pressure correction factor  $P_{cfr}$ :

$$P_{cfr} = F_{fr}^{Pc} P_{cfr}^i \tag{14}$$

The capillary pressure correction factor is computed from the composite permeability correction factor  $F_{fr}^k$  and porosity correction factor  $F_{fr}^{Pc}$  (above) according to the theory of Leverett [9]:

$$F_{fr}^{Pc} = \sqrt{\frac{F_{fr}^k}{F_{fr}^\phi}}; \quad F_{fr}^k = \sqrt{F_{lfr}^k F_{tfr}^k} \tag{15}$$

Hydrologic and geomechanical properties of the fracture zone are given in Table 2. The initial fracture apertures were computed using a cubic block conceptual model with a uniform block size of 0.5 m, assuming an initial permeability equal to the host rock permeability. The matrix component of the fracture zone will not contribute to the zone porosity or permeability.

Property	Symbol	Value
Initial Longitudinal Fracture Permeability, mD	$k_{lfr}^i$	0.01
Initial Transverse Fracture Permeability, mD	$k_{tfr}^i$	0.1
Initial Longitudinal Fracture Aperture, $\mu\text{m}$	$b_l^i$	4.3
Initial Transverse Fracture Aperture, $\mu\text{m}$	$b_t^i$	6.6
Initial Fracture Porosity	$\phi_{fr}^i$	$3.0 \times 10^{-5}$
Maximum Longitudinal Fracture Aperture, $\mu\text{m}$	$b_l^{\text{max}}$	430
Maximum Transverse Fracture Aperture, $\mu\text{m}$	$b_t^{\text{max}}$	660
Empirical Exponent Coefficient, 1/Pa	$d$	$1.0 \times 10^{-6}$

Table 2: Permeability and porosity properties for the fracture zone.

Rock	Porosity	Horizontal Permeability, mD	Vertical Permeability, mD
HP Sandstone	0.19	300	300
IP Sandstone	0.10	26.0	26.0
IP Siltstone	0.08	0.1	0.01
LP Siltstone	0.04	0.01	0.001
Overburden	0.01	0.001	0.001
Basement Rock	0.01	0.001	0.001

Table 3: Permeability and porosity properties for unfractured rock.

### *Unfractured rock*

Hydrologic properties for permeability and porosity of the unfractured rock are given in Table 3.

### *Relative permeability-saturation-capillary pressure*

Prior to CO<sub>2</sub> injection the hydrologic system will be single-phased, an aqueous phase comprising water and dissolved salt. Injection of CO<sub>2</sub> will result in a two-phased hydrologic system, having an aqueous and gas phase. The aqueous phase will comprise water, dissolved salt, and dissolved CO<sub>2</sub>. The gas phase will comprise CO<sub>2</sub> in a supercritical state and dissolved water. The relationship between effective aqueous saturation  $\bar{s}_l$  and capillary pressure  $h_{gl}$  (expressed as water equivalent head) will be that of Brooks and Corey [2].

$$\bar{s}_l = \frac{s_l - s_{lr}}{1 - s_{lr}} = \left( \frac{\Psi}{h_{gl}} \right)^\lambda \quad (16)$$

where  $\Psi$  and  $\lambda$  are Brooks and Corey function parameters,  $s_l$  is the aqueous saturation, and  $s_{lr}$  is the residual aqueous saturation.

The relationship between aqueous and gas relative permeability,  $k_{rl}$  and  $k_{rg}$ , respectively, and effective aqueous saturation will be that of Brooks and Corey (1964) [2]:

$$\begin{aligned} k_{rl} &= (\bar{s}_l)^3 \\ k_{rg} &= (1 - \bar{s}_l)^2 (1 - \bar{s}_l^2) \end{aligned} \quad (17)$$

Gas entrapment through the mechanism of nonwetting fluid entrapment will not be considered for this problem. Parameters for the capillary pressure and saturation function and the phase relative permeability and saturation functions are given in Table 4.

## **Rock Mechanics and Properties**

Geomechanical deformation will be limited to elastic behavior for the rock masses. The relationship between porosity ( $\phi$ ) and mean effective stress ( $\sigma'_M$ ) for the unfractured rock will be that of Davis and Davis (1999) [5]:

$$\phi = \phi_r + (\phi_o - \phi_r) \exp(D_\phi \sigma'_M) \quad (18)$$

The Davis-Davis porosity function parameter ( $D_\phi$ ) will be  $5 \times 10^{-8}$  1/Pa for all unfractured rocks. The mean effective stress  $\sigma'_M$  will be determined from the principal effective stresses  $\sigma'_i$  for  $i = 1, 2, 3$ ; where, the principal effective stresses will be determined from the average fluid pressure ( $s_l P_l + s_g P_g$ ), Biot's effective stress parameter  $\alpha$ , and the principal stresses (with tension being positive):

Rock	Brooks-Corey parameters		Residual aq. saturation
	$\Psi$ , m	$\lambda$	$s_{lr}$
HP Sandstone	0.4	1.2	0.07
IP Sandstone	1.0	0.8	0.06
IP Siltstone	20.0	0.8	0.06
LP Siltstone	50.0	0.8	0.06
Fracture Zone	0.085	0.65	0.01
Overburden	20.0	0.8	0.06
Basement Rock	300	0.1	0.10

Table 4: Relative permeability-saturation-capillary pressure function parameters.

Rock	Young's Modulus, GPa	Poisson's Ratio	Biot's Parameter	Bulk Density kg/m <sup>3</sup>
HP Sandstone	10	0.23	0.65	2406
IP Sandstone	15	0.23	0.65	2522
IP Siltstone	30	0.23	0.70	2547
LP Siltstone	35	0.23	0.70	2599
Fracture Zone	15	0.23	1.0	2547
Overburden	5	0.25	1.0	2637
Basement Rock	65	0.29	0.85	2637

Table 5: Rock geomechanical properties

$$\begin{aligned}\sigma'_M &= \frac{1}{3}(\phi'_1 + \phi'_2 + \phi'_3) \\ \phi'_i &= \phi_i + \alpha[s_l P_l + s_g P_g], \quad i = 1, 2, 3\end{aligned}\tag{19}$$

The relationship between intrinsic permeability and porosity for the unfractured rock will be that of Davis and Davis (1999) [5]:

$$k = k_o \exp \left[ D_k \left( \frac{\phi}{\phi_o} \right) \right]\tag{20}$$

The Davis-Davis intrinsic permeability function parameter ( $D_k$ ) will be 22.2 for all unfractured rocks. Geomechanical properties of the rocks are given in Table 5.

Rock	Matrix Thermal Conductivity, W/m K	Matrix Specific Heat, W/m K
HP Sandstone	5.9	775
IP Sandstone	5.9	775
IP Siltstone	3.2	900
LP Siltstone	3.2	900
Fracture Zone	3.2	900
Overburden	2.5	800
Basement Rock	5.0	1000

Table 6: Rock thermal properties for Problem 2a.

### Rock Thermal Properties

Non-isothermal conditions are assumed, but thermal stress are not considered. The thermal conductivity ( $\kappa_{eff}$ ) of a fluid filled rock element will be determined using an arithmetic mixing model [1]:

$$\kappa_{eff} = (1 - \phi) \kappa_m + \phi s_l \kappa_l + \phi s_g \kappa_g \quad (21)$$

where  $\kappa_m$ ,  $\kappa_l$  and  $\kappa_g$  are the thermal conductivities for the matrix, aqueous and gas phases, respectively. The specific heat of the dry rock  $(c_p)_{dry}$  will be determined from the matrix specific heat  $(c_p)_m$  and porosity:

$$(c_p)_{dry} = (1 - \phi) (c_p)_m \quad (22)$$

The matrix thermal conductivity [1] and specific heat [11] of the rocks are given in Table 6.

## 2.2 Model Comparison Reporting

This benchmark problem involves the injection of supercritical CO<sub>2</sub> into a primary lower saline reservoir with a fracture zone in the primary caprock. Geomechanical changes with CO<sub>2</sub> injection increases the permeability of the fracture zone, allowing CO<sub>2</sub> to migrate into the upper secondary reservoir. The fracture zone is offset from the injection well. A question of particular interest for this benchmark is whether the leakage of CO<sub>2</sub> through the fracture zone into the upper secondary reservoir can be detected through the vertical displacement profiles on the ground surface. The upper secondary reservoir is within temperature and pressure conditions for the CO<sub>2</sub> to remain in supercritical state; therefore, this benchmark problem is only concerned with two phases: a liquid water dominate aqueous phase and a CO<sub>2</sub> dominate gas phase. Changes to porosity and permeability of the unfractured rock and to the fracture zone from thermal stress will not be consider in this problem. The temperature of the

injected CO<sub>2</sub>, however, is lower than the host rock making heat transport and temperature dependent fluid properties a element of this problem.

### **CO<sub>2</sub> Migration into the Secondary Reservoir**

The mass rate and integral of water and CO<sub>2</sub> migrating across the top of the fracture zone shall be reported over the 30-year simulation period.

### **Gas Saturation and Fluid Pressure**

Spatial distribution profiles of gas saturation, gas pressure, and aqueous pressure shall be reported every five years during the 30-year simulation period, as a  $x$ - $z$  contour plot.

### **Porosity and Permeability**

Spatial distribution profiles of changes in porosity and intrinsic permeability shall be reported every five years during the 30-year simulation period, as a  $x$ - $z$  contour plot.

### **Vertical Displacement**

Spatial distribution profiles of ground surface vertical displacements shall be reported every five years during the 30-year simulation period, as a vertical displacement versus horizontal distance across the ground surface (i.e.,  $x$  distance).

### **Effective Stress**

Spatial distribution profiles of changes in the  $x$ - $z$  components of effective stress ( $\Delta\sigma'_x$ ,  $\Delta\sigma'_z$ ) shall be reported every five years during the 30-year simulation period, as a  $x$ - $z$  contour plot.

## **3 Modeling approach**

It is unlikely that any participating group will be able to obtain an analytical solution (or converged numerical solution) taking into account all physical and chemical processes in the system. Certain approximations must therefore be introduced, and these approximations will likely impact the answers to the comparison results. It is therefore paramount that each modeling group carefully details the approximations they have introduced, be it in upscaling, discretization, or treatment of physical processes.

## References

- [1] A. C. Aplin, A. J. Fleet, and J. H. S. Macquaker. Muds and mudstones: Physical and fluid-flow properties. *Geological Society London, Special Publications*, 158:45–60, 1999.
- [2] R. J. Brooks and A. T. Corey. Hydraulic properties of porous media. *Hydrology Papers*, 3, 1964.
- [3] A. Cavanagh and P. Ringrose. Simulation of CO<sub>2</sub> distribution at the In Salah storage site using high-resolution field-scale models. *Energy Procedia*, 4:3730—3737, 2011.
- [4] H. Class, A. Ebigbo, R. Helmig, H. K. Dahle, J. M. Nordbotten, M. A. Celia, P. Audigane, M. Darcis, J. Ennis-King, Y. Fan, B. Flemisch, S. E. Gasda, M. Jin, S. Krug, D. Labregere, A. N. Beni, R. J. Pawar, A. Sbai, S. G. Thomas, L. Trenty, and L. Wei. A benchmark study on problems related to CO<sub>2</sub> storage in geologic formations. *Computational Geosciences*, 13(4):409–434, 2009.
- [5] J. P. Davis and D. K. Davis. Stress-dependent permeability: characterization and modeling. *Society of Petroleum Engineers*, pages SPE–56813, 1999.
- [6] J. M. Nordbotten, B. Flemisch, S. E. Gasda, H. M. Nilsen, Y. Fan, G. E. Pickup, B. Wiese, M. A. Celia, H. K. Dahle, G. T. Eigestad, and K. Pruess. Uncertainties in practical simulation of CO<sub>2</sub> storage. *International Journal of Greenhouse Gas Control*, 2012. in press.
- [7] K. Pruess, Julio García, T. Kavscek, C. Oldenburg, J. Rutqvist, C. Steefel, and T. Xu. Code intercomparison builds confidence in numerical simulation models for geologic disposal of CO<sub>2</sub>. *Energy*, 29:1431–1444, 2004.
- [8] J. Rutqvist, D. W. Vasco, and L. Myer. Coupled reservoir-geomechanical analysis of CO<sub>2</sub> injection and ground deformations at In Salah, Algeria. *International Journal of Greenhouse Gas Control*, 4:225–230, 2010.
- [9] J. Rutqvist, Y.-S. Wu, C.-F. Tsang, and G. Bodvarsson. A modeling approach for analysis of coupled multiphase fluid flow, heat transfer, and deformation in fractured porous media. *International Journal of Rock Mechanics & Mining Sciences*, 39:429–442, 2002.
- [10] D. W. Vasco, A. Ferretti, and F. Novali. Reservoir monitoring and characterization using satellite geodetic data: Interferometric synthetic aperture radar observations from the Krechba field, Algeria. *Geophysics*, 73(6):WA113–WA122, 2008.
- [11] D. W. Waples and J. S. Waples. A review and evaluation of specific heat capacities of rocks, minerals, and subsurface fluids. part 1: Minerals and nonporous rocks. *Natural Resources Research*, 13(2):97–122, 2004.